A kinetic analysis of protein transport through the anthrax toxin channel

Daniel Basilio,[1,2] Paul K. Kienker,[1] Stephen W. Briggs,[2] and Alan Finkelstein[1,2]

[1]Department of Physiology and Biophysics and [2]Dominick P. Purpura Department of Neuroscience, Albert Einstein College of Medicine, Bronx, NY 10461

Anthrax toxin is composed of three proteins: a translocase heptameric channel, $(PA_{63})_7$, formed from protective antigen (PA), which allows the other two proteins, lethal factor (LF) and edema factor (EF), to translocate across a host cell's endosomal membrane, disrupting cellular homeostasis. $(PA_{63})_7$ incorporated into planar phospholipid bilayer membranes forms a channel capable of transporting LF and EF. Protein translocation through the channel can be driven by voltage on a timescale of seconds. A characteristic of the translocation of LF_N, the N-terminal 263 residues of LF, is its S-shaped kinetics. Because all of the translocation experiments reported in the literature have been performed with more than one LF_N molecule bound to most of the channels, it is not clear whether the S-shaped kinetics are an intrinsic characteristic of translocation kinetics or are merely a consequence of the translocation in tandem of two or three LF_Ns. In this paper, we show both in macroscopic and single-channel experiments that even with only one LF_N bound to the channel, the translocation kinetics are S shaped. As expected, the translocation rate is slower with more than one LF_N bound. We also present a simple electrodiffusion model of translocation in which LF_N is represented as a charged rod that moves subject to both Brownian motion and an applied electric field. The cumulative distribution of first-passage times of the rod past the end of the channel displays S-shaped kinetics with a voltage dependence in agreement with experimental data.

INTRODUCTION

The toxin produced by *Bacillus anthracis*, the causative agent of anthrax, consists of three separate monomeric proteins. Two of them, edema factor (EF; 89 kD) and lethal factor (LF; 90 kD), are enzymes that produce their toxic effects upon gaining access to the cytosol of the target cell. Access is gained through the agency of the third protein, protective antigen (PA; 83 kD), which provides a channel for their entry into the cytosol from an intracellular acidic vesicle compartment in which they find themselves after receptor-mediated endocytosis. (For a general review of anthrax toxin, see Young and Collier, 2007.) The channel formed by PA, $(PA_{63})_7$, is a heptamer of the 63-kD fragment left after the cleavage of a 20-kD fragment from the N-terminal end of PA. (An octameric channel can also be formed [Kintzer et al., 2009].) This channel is mushroom shaped with a long (100 Å) 14-stranded β-barrel stem (Fig. 1; Benson et al., 1998; Nassi et al., 2002; Nguyen, 2004; Katayama et al., 2008); near the entry to the stem is a ring of phenylalanines dubbed the Φ clamp (Krantz et al., 2005). The seven binding sites for EF and LF reside in the mushroom cap, and up to three molecules of EF and/or LF can simultaneously occupy these sites (Cunningham et al., 2002;
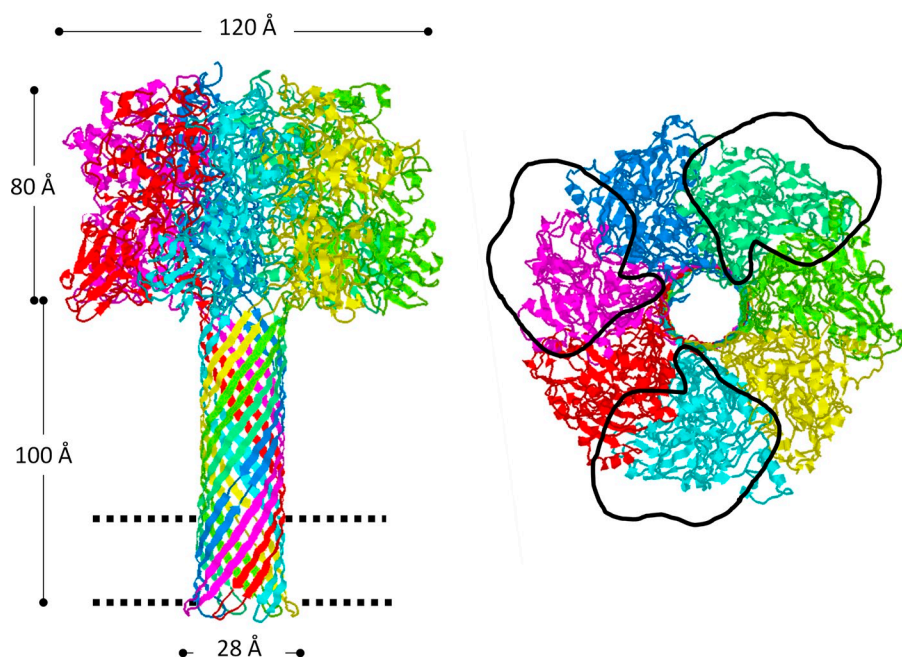
Mogridge et al., 2002; Pimental et al., 2004; Young and Collier, 2007). The ligand-binding site spans the intersection between two PA_{63} subunits; steric constraints restrict the number of ligands bound to three (Fig. 1). EF and LF can be driven by voltage and pH gradients through $(PA_{63})_7$ channels reconstituted in planar phospholipid bilayer membranes (Zhang et al., 2004a,b; Krantz et al., 2005, 2006; Basilio et al., 2009; Finkelstein, 2009), although most of these experiments, as the ones described in this paper, were performed with LF_N, the 263-residue N-terminal portion of LF that binds to the ligand-binding sites (Young and Collier, 2007).

A characteristic of the translocation of LF_N through the $(PA_{63})_7$ channel is its nonexponential S-shaped or sigmoidal kinetics (Fig. 2). That is, after the voltage step, there is a lag time with minimal conductance increase followed by a more rapid increase. In general, this sort of S-shaped kinetics is expected for a process with multiple sequential steps, even if the individual steps have exponential kinetics. Under the conditions of the experiments reported in the literature (e.g., Zhang et al., 2004b; Krantz et al., 2005, 2006) as well as those for the experiment depicted in Fig. 2, it is likely that most of the $(PA_{63})_7$ channels bound two or three LF_Ns (see Theory section). If this is so, it is possible that

Figure 1. Structure of the $(PA_{63})_7$ channel. The figure on the left was created from the PA channel atomic model (Protein Data Bank accession no. 1V36) reported by Nguyen (2004). The parallel dashed lines indicate the thickness of the hydrophobic interior of the phospholipid bilayer. The figure on the right is a top view of this structure. The three black outlines are LF_Ns and are placed where they are presumed to bind to the mushroom cap of the channel (Melnyk et al., 2006). Note that even though there are seven binding sites in the cap, only three LF_Ns can be accommodated.

the S-shaped kinetics of translocation are solely caused by this and are not an intrinsic characteristic of the kinetics of translocation. Before one can make a quantitative kinetic model of translocation, it is essential to determine the translocation kinetics of a single LF_N molecule. In this paper, we address this issue both at the macroscopic and single-channel level. We report that with only one LF_N bound to the channel, both the macroscopic

Figure 2. The S-shaped kinetics of LF_N translocation through the $(PA_{63})_7$ channel. After the $(PA_{63})_7$-induced conductance had reached a more or less steady state, LF_N (with the N-terminal His_6 tag removed) was added (at the arrow) to the cis-side to a concentration of 6 nM, resulting in a rapid fall in conductance. LF_N (along with $(PA_{63})_7$) was then perfused out of the cis-compartment (during the ~4-min break in the record); the conductance increased only slightly over this time. When the voltage was stepped from 20 to 45 mV, there was an S-shaped rise of conductance to a value comparable with that before the addition of LF_N, and it remained at that value when the voltage was stepped back from 45 to 20 mV. The rate of conductance rise directly reflects the rate of translocation of LF_N; i.e., the rate of its traversing the channel and exiting into the trans-solution. This figure was adapted from Fig. 2 of Finkelstein (2009).

and single-channel experiments gave S-shaped kinetics, that they were in quantitative agreement with each other, and, as might be expected, their kinetics of translocation were faster than those obtained in experiments with multiple LF_N occupancy. In addition, we present a simple drift-diffusion model of translocation in which LF_N is represented as a charged rod that moves under the combined influence of random thermal motion and an applied electrical potential difference. This model adequately accounts for the S-shaped kinetics and their voltage dependence.
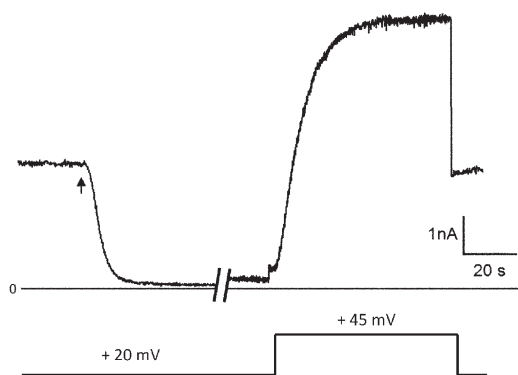
MATERIALS AND METHODS

Theory

Distribution of the number of LF_Ns bound to the channel. When a $(PA_{63})_7$ channel is blocked at 20 mV by LF_N (the starting situation in our experiments), that channel remains blocked almost all of the time, only rarely flickering open (Krantz et al., 2005). Assuming that the channel can be blocked with only one LF_N bound to it, and then given the fraction of channels that are unblocked, the distribution of the number of LF_Ns bound to the channel can be calculated as described below.
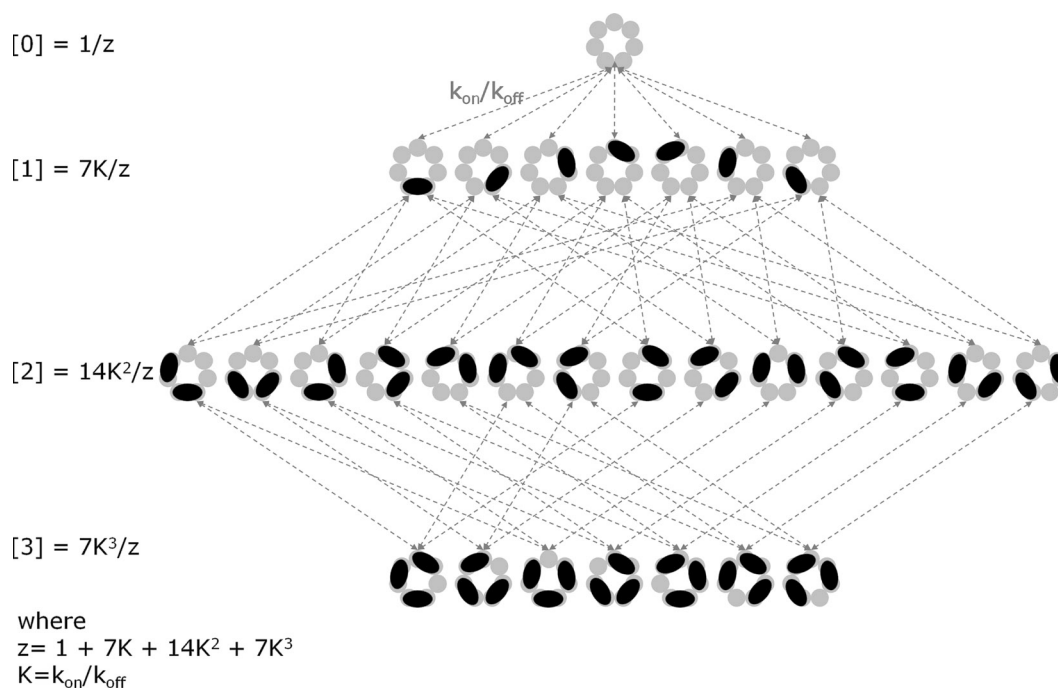
Although there are seven potential binding sites for LF_N, maximally only three can be occupied (Fig. 1; Cunningham et al., 2002; Mogridge et al., 2002; Pimental et al., 2004). Let k_{on} (which depends on the concentration of LF_N) be the on-rate constant for a given site, and let k_{off} be the off-rate constant. We assume, as shown for the whole LF (Elliott et al., 2000; Neumeyer et al., 2006), that these rate constants are independent of the number of sites occupied; therefore, at equilibrium the transitions between the different occupied states (Fig. 3) are characterized by the following set of equations:

$$7k_{on}\,[0] = k_{off}\,[1],$$

$$4k_{on}\,[1] = 2k_{off}\,[2],$$

$[0] = 1/z$

k_{on}/k_{off}

$[1] = 7K/z$

$[2] = 14K^2/z$

$[3] = 7K^3/z$

where
$z = 1 + 7K + 14K^2 + 7K^3$
$K = k_{on}/k_{off}$

Figure 3. Illustration of all the possible ways that the seven binding sites on the $(PA_{63})_7$ channel can be occupied by LF_N. The ring of seven gray circles represents the $(PA_{63})_7$ channel, and the black oval represents LF_N. Note that when LF_N is bound to the channel, it occupies two adjacent subunits. k_{on} is the rate constant for binding of LF_N to two subunits, and k_{off} is the dissociation rate. (k_{on} is directly proportional to the concentration of LF_N.) The arrows indicate the binding and unbinding transitions between each of the states. [0], [1], [2], and [3] are the fractions of channels occupied by zero, one, two, and three LF_Ns, respectively.

$$1.5k_{on} [2] = 3k_{off} [3], \text{ and}$$

$$[0] + [1] + [2] + [3] = 1,$$

where [0], [1], [2], and [3] are the fractions of channels occupied by zero, one, two, and three LF_Ns, respectively. Solving these equations, we obtain

$$\begin{aligned} [0] &= 1/z, \\ [1] &= 7K/z, \\ [2] &= 14K^2/z, \text{ and} \\ [3] &= 7K^3/z, \end{aligned} \quad (1)$$

where

$$K = k_{on}/k_{off} \text{ and}$$
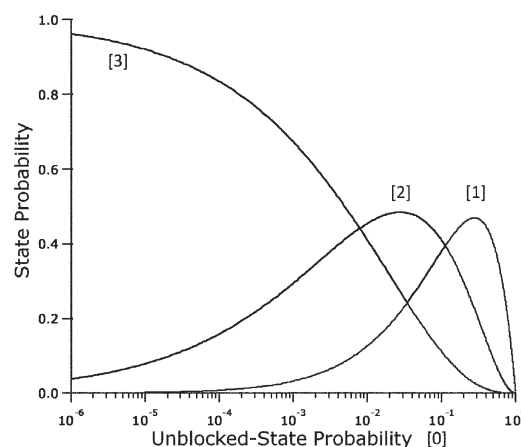
$$z = 1 + 7K + 14K^2 + 7K^3.$$

Given [0], which is the experimentally observed quantity, we can solve for K and thus determine [1], [2], and [3]. Plots of [1], [2], and [3] as a function of [0] are shown in Fig. 4.

Drift-diffusion model. As a first approximation, the voltage-dependent translocation of LF_N through the $(PA_{63})_7$ channel can be formally modeled as a drift-diffusion process for a rod that, starting from a reflecting boundary at $x = 0$, diffuses until it reaches an absorbing boundary at $x = L$. Here, x is a coordinate that describes the length of LF_N that has moved past the cis-end of the channel (Lubensky and Nelson, 1999). Thus, $x = 0$ when LF_N is just entering the cis-end of the channel, $x = L$ when LF_N is leaving the channel at the trans-end, and L represents the extended length of LF_N

plus the channel length. The choice of boundary types means that LF_N can exit the channel at the trans-end but not at the cis-end. The probability density, $p(x, t)$, for the rod being at position x at time t is given by the Fokker-Planck equation

$$\partial p/\partial t = -v\partial p/\partial x + D\partial^2 p/\partial x^2 \quad (2)$$

together with the initial condition and boundary conditions, where v is the drift velocity and D is the diffusion coefficient. The probability that LF_N has exited at the trans-end of the channel, as a function of time, corresponds to the cumulative distribution of

Figure 4. The calculated fraction of channels occupied by one, two, or three LF_Ns ([1], [2], and [3]) as a function of the fraction of channels unoccupied by LF_N ([0]).

first-passage times at the absorbing boundary, $W(\Omega, t)$. (This is analogous to the normalized conductance versus time in the data figures.) This probability distribution can be calculated from Eq. 2 as an infinite sum of orthogonal eigenfunctions (Hinkel and Mahnke, 2007); for our purposes, we found it acceptable to truncate the sum after 10^6 terms. (The moments of the first-passage time distribution can be calculated using Laplace transforms; e.g., see the solution of Berezhkovskii and Gopich [2003] for somewhat different boundary conditions.)

The Péclet number, Ω, a dimensionless parameter that represents the relative importance of drift versus diffusion, will prove useful as a way to quantify the shape of the unblocking curves—that is, how steeply sigmoidal they are. It is defined by
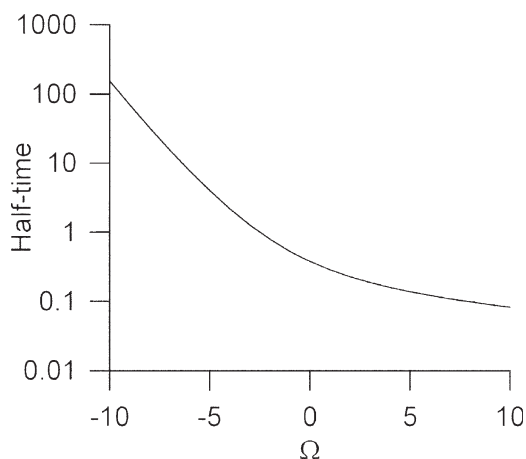
$$\Omega = vL/D. \tag{3}$$

As Ω increases, $W(\Omega, t)$ becomes more steeply sigmoidal; for large, negative Ω (approximately less than or equal to -6), $W(\Omega, t)$ approximates a single-exponential relaxation to $W(\Omega, \infty) = 1$, as the initial lag time becomes short relative to the overall timescale of translocation. (More properly, W is a function of the dimensionless time tD/L^2, but we will write t for simplicity.)

We can relate Ω to the applied transmembrane voltage, V, as follows. Suppose that the translocating LF_N has on average n positive charges moving through the voltage drop at any given time. (Following Basilio et al. [2009], we suppose that the acidic groups of LF_N within the channel are uncharged.) Assuming a constant field, the electrophoretic drift velocity is $v = unFV/\ell$, where u is the mobility, F is the Faraday constant, and ℓ is the channel length. The diffusion coefficient can be written as $D = uRT$, where R is the gas constant and T is the absolute temperature. Substituting into Eq. 3 gives

$$\Omega = nVFL/RT\ell. \tag{4}$$

Each model $W(\Omega, t)$ curve can be described by two parameters, u and Ω. For a given mobility, the rise of $W(\Omega, t)$ with time becomes faster, and thus the half-times become shorter, with increasing Ω (Fig. 5). We sometimes found it more convenient to express $W(\Omega, t)$ in terms of $t_{1/2}$ (which is proportional to $1/u$) and Ω. The half-time can be determined directly from the data curve (normalized conductance vs. time). To facilitate the fitting of Ω, we used a rescaled time variable for each curve, $t' = t/t_{1/2}$, to make the model and data curves superimpose at

a value of $1/2$ when $t' = 1$. We then plotted a family of model curves for various values of Ω and visually determined which one best matched a given data curve. For this, we emphasized the earlier part of the curve on the rationale that the later part was more likely to be contaminated by channel-gating effects. All analysis routines were written using the program Igor Pro (WaveMetrics, Inc.).

Protein purification

Wild-type (WT) PA (83 kD) and LF_N (residues 1–263 of LF, containing the N-terminal pET15b-encoded thrombin-cleavable His$_6$ tag [Merck]) were expressed recombinantly and purified as described previously (Benson et al., 1998; Zhang et al., 2004a). In some experiments, the N-terminal His$_6$ tag was removed as described by Zhang et al. (2004a), and we refer to this as WT LF_N. The heptameric prepore form of PA_{63} was prepared by nicking PA_{83} with trypsin and purifying the PA_{63} heptamer from the smaller 20-kD fragment using anion-exchange chromatography (Cunningham et al., 2002).

Planar lipid bilayers

For the macroscopic experiments, bilayers were formed by the brush technique (Mueller et al., 1963) across a 300-μm diameter aperture polystyrene cup (Warner Instruments); the single-channel experiments were performed in a polystyrene cup with a hole diameter of 50 μm manufactured in house as described previously (Wonderlin et al., 1990). Membranes separated two compartments of 1 ml containing symmetric buffered solutions of 100 mM KCl, 5 mM potassium succinate, and 1 mM EDTA, pH 5.5, which could be stirred by small magnetic bars. Agar salt bridges (3 M KCl and 3% agar) linked Ag/AgCl electrodes in saturated KCl baths to the cis- and trans-compartments. The membrane-forming solution was 3% diphytanoyl-phosphatidylcholine (Avanti Polar Lipids, Inc.) in n-decane, and membrane formation was monitored both visually and by capacitance. All experiments were performed under voltage-clamp conditions with a Bilayer Clamp (BC-535C; Warner Instruments); voltages are those of the cis-solution (to which protein was added) with respect to the trans-solution, which was held at virtual ground. Current responses were filtered at 1 kHz by a low-pass eight-pole Bessel filter (Warner Instruments), recorded by computer via an analog-to-digital converter (NI USB-6211; National Instruments) at 20 Hz using IGOR NIDAQ Tools MX 1.0 and IGOR 6.0.3.1 (WaveMetrics, Inc.), and confirmed by a chart recorder (DMP-4B Physiograph; Narco Bio-Systems Inc.).

$(PA_{63})_7$ channel formation, LF_N conductance block, and translocation

Macroscopic experiments. After membrane formation, PA_{63} prepore heptamer was added to the cis-compartment (to a final concentration of ~1 ng/ml [~2 pM]), which was held at a voltage, V, of 20 mV with respect to the trans-compartment. After the conductance consequent to $(PA_{63})_7$ channel formation had reached a more or less constant level, WT LF_N or His$_6$-LF_N was added to the cis-compartment. The progress of LF_N binding to $(PA_{63})_7$ channels and blocking them was monitored by the continuous fall of conductance. With the exception of those experiments in which we strived to have no more than one LF_N bound to the channel, ~95% of the conductance was blocked by LF_N (final concentration of ~3 nM) at 20 mV before translocation experiments were begun. After LF_N conductance block of $(PA_{63})_7$ channels was complete, excess ligand was removed from the cis-compartment by perfusion using a bilayer perfusion system (BPS-2; Warner Instruments) coupled to a peristaltic pump (Buchler). The exchange of 10 vol was accomplished in 3 min while V was held constant at 20 mV. After this, V was stepped to a larger voltage (45–60 mV), and the rate of LF_N

Figure 5. The dimensionless half-time for translocation (tD/L^2) as a function of the Péclet number, Ω, calculated from the drift-diffusion model.

translocation was determined, as reflected in the rate of conductance rise caused by LF_N traversing the channel and exiting into the trans-solution. In general, the final conductance was ≥90% of the conductance before blocking by LF_N.

Single-channel experiments. PA_{63} prepore heptamer was added to the cis-compartment (to a final concentration of ~10 pg/ml [~20 fM]), which was held at a *V* of 20 mV with respect to the trans-compartment. After ~20 min. a single channel appeared, and His_6-LF_N was added to the cis-compartment (final concentration of ~30 pM). Typically, there was an ~1-min waiting time to see a blocking event. After 5 s in the blocked state, the voltage was stepped from 20 to either 48 mV in one experiment or 50 mV in another experiment until the single-channel current reappeared (that is, His_6-LF_N had been translocated through the channel). The voltage was then stepped back to 20 mV, and this maneuver was repeated (Fig. 6, inset). Under this protocol, one can assume that generally only one molecule of His_6-LF_N was translocated, given that the mean time of blocking was five times shorter than the waiting time before the voltage step. The interval between the voltage step (from 20 to 48 or 50 mV) and the reopening of the channel is the lag time (Δt) used to build the survival curve presented in Fig. 6; this curve, by normalizing and inverting, is readily converted to a cumulative probability distribution of translocation times as depicted in Fig. 7.
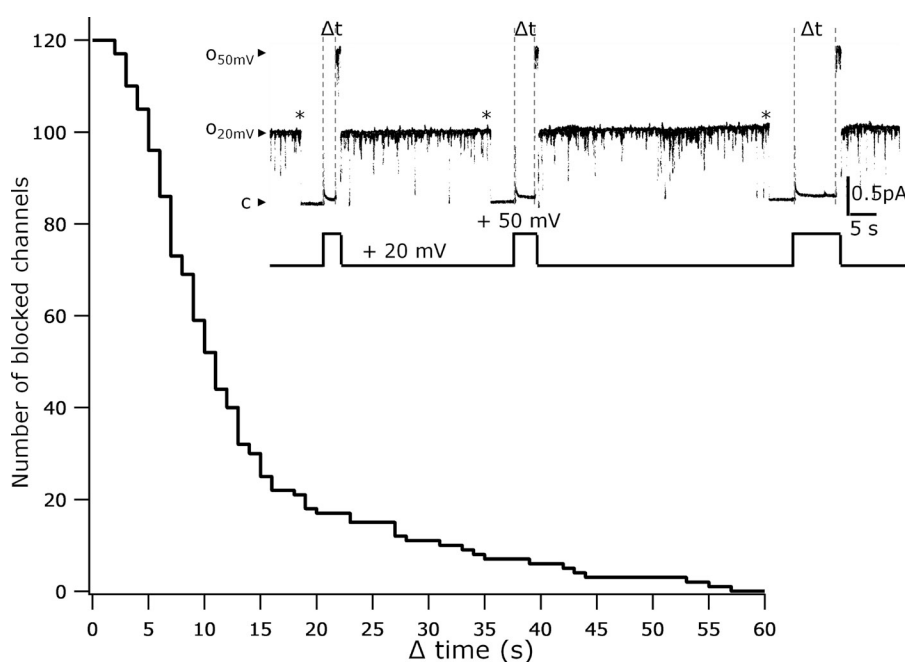
RESULTS

Comparison of macroscopic and single-channel experiments

We were able to determine the translocation kinetics of a single LF_N molecule through the $(PA_{63})_7$ channel using either macroscopic or single-channel experiments; these results are summarized in Fig. 7. For the macroscopic experiments, we used such a low concentration of LF_N that most channels were not blocked, and the vast majority of blocked channels had only one LF_N
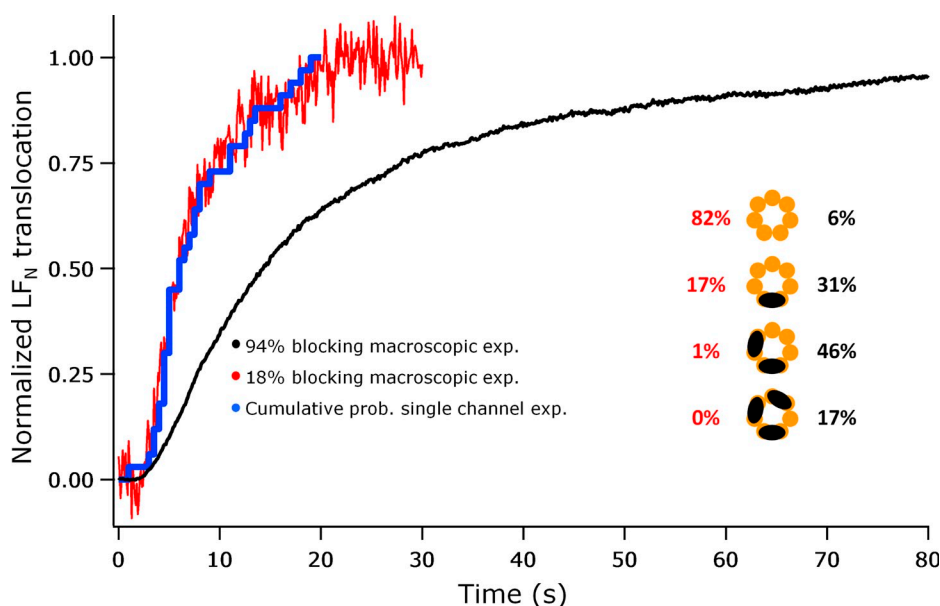
bound. For the single-channel experiments, the voltage was pulsed to initiate translocation so soon after channel blocking that translocation was completed before there was time for another LF_N molecule to bind. Consider first the macroscopic experiment, in which only 18% of the channels were blocked by His_6-LF_N (82% unblocked). From Eq. 1, this means that in the population of blocked channels, almost all of them had only one His_6-LF_N bound to them (94.4% with one bound, 5.5% with two bound, and 0.1% with three bound). Thus, the kinetics are essentially those for channels having one bound His_6-LF_N and have a half-time of 6 s. Turning now to the cumulative probability distribution of the translocation times from single-channel experiments, in which virtually all of the translocation events occurred with only one His_6-LF_N bound to the channel (see Materials and methods section), we note that it is superimposable on the macroscopic result. (The survival plot depicted in Fig. 6 was obtained by stepping the voltage from 20 to 48 mV instead of to 50 mV; the half-time at 48 mV was 8 s instead of 6 s at 50 mV.) Finally, we see that when 94% of the channels were blocked by His_6-LF_N (6% unblocked), translocation was, as expected, slower than when only 18% of the channels were blocked (half-time of 14 s compared with 6 s). In this case, according to Eq. 1, within that population of blocked channels, 33% had one His_6-LF_N bound, 49% had two bound, and 18% had three bound. Thus, the kinetics were significantly weighted by channels that had more than one His_6-LF_N bound.

Fitting the drift-diffusion model to the data

We next used the drift-diffusion model to quantitate the sigmoidal shape of the translocation kinetics. The single

Figure 6. A survival plot of the number of channels that are still blocked by His_6-LF_N (that is, His_6-LF_N has not yet translocated through them) as a function of time (Δt) after the voltage was stepped from 20 to 48 mV. A representative single-channel record from which the plot was generated is shown in the inset. (In this single-channel record, the voltage was stepped to 50 instead of to 48 mV.) With the voltage held at 20 mV, an open channel became blocked by His_6-LF_N (present in the cis-solution) at the first asterisk. After 5 s, the voltage was stepped to 50 mV, and after time Δt, the channel became unblocked. The voltage was then stepped back to 20 mV. After ~25 s, the channel became blocked again, and the voltage was stepped to 50 mV, etc. The arrowheads mark the current level of the closed channel (c), the open channel at 20 mV (O_{20}), and the open channel at 50 mV (O_{50}).

Figure 7. The translocation kinetics of His$_6$-LF$_N$ through the (PA$_{63}$)$_7$ channel determined from macroscopic experiments compared with that determined from single-channel experiments. The protocol before stepping the voltage from 20 to 50 mV in the macroscopic experiments (the red and black curves) was the same as that described in the legend to Fig. 2. The cumulative probability distribution of translocation times (blue curve) was obtained from a survival curve (derived from single-channel experiments), such as that shown in Fig. 6, except that in this case the voltage was stepped from 20 to 50 mV (instead of to 48 mV). In the macroscopic experiment depicted by the red curve, the concentration of His$_6$-LF$_N$ was so small that it only produced an 18% fall in conductance. T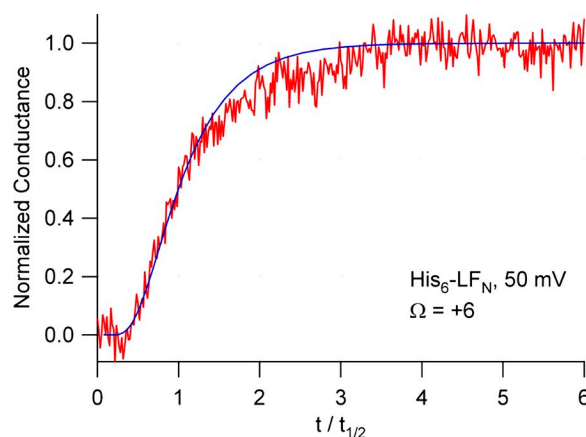hus, virtually all of the blocked channels had only one His$_6$-LF$_N$ bound to them. Note that the kinetics are identical to those obtained from the single-channel experiment (blue curve). In the macroscopic experiment depicted by the black curve, the concentration of His$_6$-LF$_N$ was much larger, producing a 94% fall in conductance. In this case, ~70% of the blocked channels had two or three His$_6$-LF$_N$s bound to them (Fig. 4). Note that the rate of unblocking in this case was, as expected, slower than in the case when the blocked channels contained only one His$_6$-LF$_N$. The cartoon indicates the percentage of channels that have zero, one, two, and three His$_6$-LF$_N$s bound to them when there was an 18% fall in conductance produced by His$_6$-LF$_N$ (red numbers) and when there was a 94% fall in conductance (black numbers).

His$_6$-LF$_N$ (18% block) macroscopic data at 50 mV from Fig. 7 are replotted in Fig. 8 (red curve) with the time axis normalized by the half-time. The superimposed blue curve is the cumulative first-passage time distribution $W(\Omega, t')$ calculated for $\Omega = 6$.
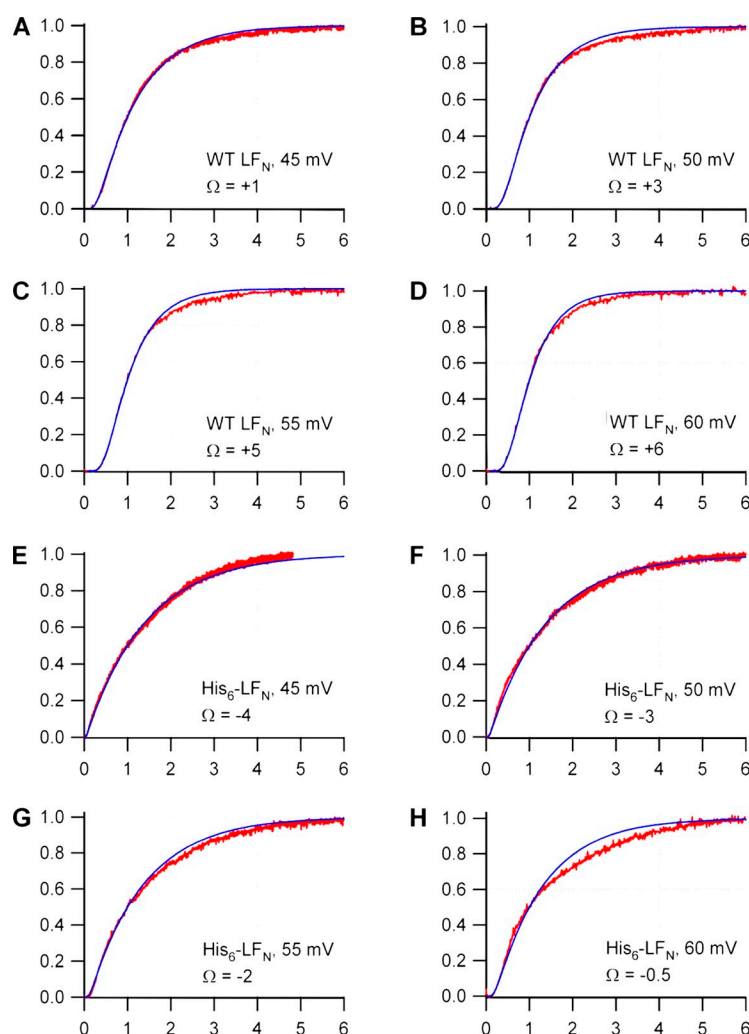
We have generally observed that the translocation of His$_6$-LF$_N$ is significantly slower than that of WT LF$_N$ (which has the His$_6$ tag removed). (Indeed, we took advantage of this property to facilitate the measurement of the lag time in the single-channel translocation experiments.) To confirm this, we compared the translocation kinetics of WT LF$_N$ and His$_6$-LF$_N$ on the same membrane using our standard ~95% block condition. And indeed, at a given voltage, $t_{1/2}$ for His$_6$-LF$_N$ is greater than that for WT LF$_N$ (see Fig. 11). Fig. 9 shows the normalized conductance plotted against normalized time ($t/t_{1/2}$) for WT LF$_N$ (A−D) and His$_6$-LF$_N$ (E−H) over a range of voltages. The superimposed blue curves are $W(\Omega, t')$ for the best fitted values of Ω. We see that the translocation kinetics of WT LF$_N$ are more sigmoidal (i.e., have more positive Ω) than those of His$_6$-LF$_N$.

An examination of the voltage dependence of the fitted Ω values (Fig. 10) supports the prediction of Eq. 4 that Ω should increase linearly with V and indicates that the quantity nL/ℓ is in the range from 6 (His$_6$-LF$_N$) to 9 (WT LF$_N$). However, the prediction that $\Omega = 0$ when $V = 0$ is not satisfied (assuming that we can extrapolate the linear trend). We can salvage the theory by supposing that the fixed charges in the (PA$_{63}$)$_7$ channel create a

local electrostatic potential, more negative at the cis-end than at the trans-end. This would effectively shift the voltage sensed by LF$_N$ to more negative values. (Of course, thermodynamics would not allow this internal potential to drive LF$_N$ translocation from the trans- to the cis-solution at $V = 0$, but escape to the cis-solution is outside the scope of the present discussion.) Extrapolation of the lines in Fig. 10 indicates that $\Omega = 0$ when $V = 41$ mV (WT LF$_N$) or 63 mV (His$_6$-LF$_N$), so the effective
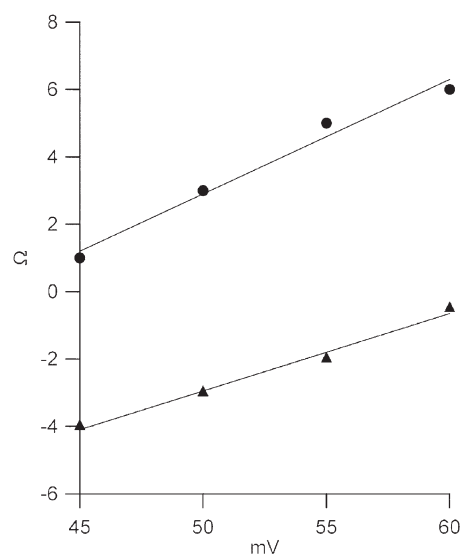

Figure 8. The fit of the drift-diffusion model to the translocation kinetics of a single His$_6$-LF$_N$ molecule. Drift-diffusion model, blue curve; single His$_6$-LF$_N$ molecule, red curve. The red curve is the same as that in Fig. 7, except that the time axis has been normalized by the half-time.
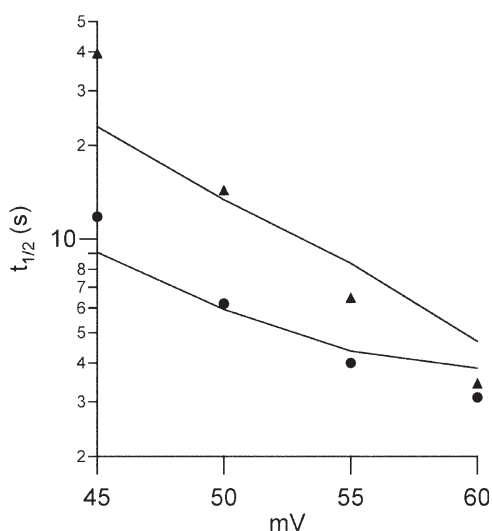
Figure 9. The fit of the drift-diffusion model to the translocation kinetics of WT LF_N and His_6-LF_N over a range of voltages. Drift-diffusion model, blue curves; WT LF_N and His_6-LF_N, red curves. The ordinates are normalized to the conductance before the addition of WT LF_N or His_6-LF_N, and the abscissas are normalized time ($t/t_{1/2}$). All of the experiments were performed on the same membrane. The experimental procedure was the same as that described in Fig. 2, except after translocation was completed, WT LF_N or His_6-LF_N was again added to the cis-solution, and the protocol was repeated. At each voltage, the experiment with WT LF_N was followed by that with His_6-LF_N. In contrast to the experiment depicted in Fig. 8, where the addition of His_6-LF_N caused a conductance drop of 18%, the addition of WT LF_N or His_6-LF_N here caused a drop of ~95%; thus, most of the channels bound two or three LF_Ns.

offset would be the opposite voltage. Although we can rationalize the negative sign of the offset voltage (see Discussion), it is not clear why His_6-LF_N and WT LF_N should have different offsets.

Fig. 11 shows $t_{1/2}$ as a function of voltage for both WT LF_N and His_6-LF_N. The fitted curves were constructed by taking the Ω values fitted in Fig. 9 and using the dependence of $t_{1/2}$ on Ω, inherent in the drift-diffusion model (Fig. 5), to determine the voltage dependence. The ratio D/L^2 was then adjusted to fix the absolute timescale. Based on its more negative Ω values, His_6-LF_N is predicted to have slower translocation kinetics than WT LF_N, which it indeed has, but the predicted slowing is substantially greater than is actually observed. Thus, we allowed His_6-LF_N to have a larger diffusion coefficient, D, than WT LF_N. Supposing that for the highly blocked condition there are on average about two LF_N molecules bound per channel (Fig. 4), we take L to represent twice the extended length of LF_N ($L = \sim2,000$ Å); then, the fitted curves in Fig. 11 correspond to $D = 1 \times 10^{-11}$ cm^2/s for WT LF_N and 4×10^{-11} cm^2/s for His_6-LF_N. Note that these are very slow diffusion coefficients (see Discussion).

Figure 10. The voltage dependence of Ω. The Ω values are taken from Fig. 9. The circles are WT LF_N, and the triangles are His_6-LF_N. The points are fit to Eq. 4 (allowing for an offset voltage), with nL/ℓ = 8.7 for WT LF_N and 5.9 for His_6-LF_N. Extrapolation of the lines indicates that at $\Omega = 0$, $V = 41$ mV for WT LF_N and 63 mV for His_6-LF_N.

Figure 11. The half-time of translocation as a function of voltage. The values for WT LF$_N$ (circles) and His$_6$-LF$_N$ (triangles) are from the experiments described in Fig. 9. Note that at every voltage, the rate of translocation of His$_6$-LF$_N$ is slower than that of WT LF$_N$ but that the rates tend to converge as the voltage increases. Thus, His$_6$-LF$_N$ $t_{1/2}$/WT LF$_N$ $t_{1/2}$ = 3.3, 2.3, 1.6, and 1.1 for V = 45, 50, 55, and 60 mV, respectively. The fitted curves were calculated from the drift-diffusion model as described in the Results section.

DISCUSSION

The first requirement in any attempt to model the steps involved in the translocation of LF$_N$ through the (PA$_{63}$)$_7$ channel—unfolding of the protein, its passage through the Φ clamp on its way to entering the stem (Fig. 1), and its movement down the 100-Å-long stem—is knowledge of the translocation kinetics. The kinetics were obtained from experiments such as that depicted in Fig. 2, in which after the channel was blocked by LF$_N$ at some small positive voltage (e.g., 20 mV), the voltage was stepped to a larger positive value, and the rate of channel unblocking was taken as a measure of the kinetics of LF$_N$ translocation. However, because the (PA$_{63}$)$_7$ channel can bind up to three LF$_N$ molecules (Melnyk et al., 2006) and all of these must pass through the channel in tandem before the channel is unblocked, the intrinsic kinetics of LF$_N$ translocation will be obscured if more than one LF$_N$ is bound. In point of fact, all of the translocation experiments reported in the literature (e.g., Zhang et al., 2004b; Krantz et al., 2005, 2006), including almost all of our own experiments, were performed with most of the channels containing two or three bound LF$_N$s. As a result, it is not clear whether the S-shaped kinetics seen in those experiments (e.g., Fig. 2) are simply a consequence of having to drive two or three LF$_N$s through each channel before it is unblocked or whether the intrinsic translocation kinetics of LF$_N$ are S shaped.

In this paper, we have addressed and answered this question both at the macroscopic and single-channel level. In the former case, we added a sufficiently small amount of His$_6$-LF$_N$ such that only 18% of the channels were blocked, and of those, only 5.6% (i.e., 1/18; Fig. 7) had more than one His$_6$-LF$_N$ bound. In the latter case, the LF$_N$ concentration was such that generally only one His$_6$-LF$_N$ molecule was translocated when the voltage was stepped from 20 to 48 or 50 mV (see Materials and methods, Single-channel experiments). By both methods, we found that the intrinsic translocation kinetics of His$_6$-LF$_N$ were S shaped (Figs. 6 and 7), and, gratifyingly, the macroscopic and single-channel kinetics were identical (Fig. 7). That the translocation kinetics are S shaped is not surprising. Given the numerous sequential steps that must be taken before LF$_N$ has fully traversed the (PA$_{63}$)$_7$ channel, the only circumstance that would give rise to exponential, rather than S-shaped, kinetics would be if one of those steps were so much slower than all the others that it became rate limiting.

To represent these numerous sequential steps, we have considered a highly simplistic drift-diffusion model. Although the model omits many factors that could potentially be important, we feel that it is useful to see just how far it can take us, in the hope that it distills the essence of the phenomenon. We have therefore represented the translocation of LF$_N$ from cis to trans through the stem of (PA$_{63}$)$_7$ (Fig. 1) as the one-dimensional movement of a charged Brownian rod under the combined influence of random thermal motion and an applied electrical potential difference (V). More precisely, the position of the rod represents the extended length of the LF$_N$ chain that has passed the cis-entrance of the channel. The rod starts at a reflecting boundary (when LF$_N$ is just entering the channel at the cis-end) and travels a distance, L, to an absorbing boundary (when LF$_N$ leaves the channel at the trans-end). Thus, L represents the extended length of LF$_N$ (plus the much shorter channel length, ℓ). Using this model, we have calculated the cumulative distribution of the first-passage times at the absorbing boundary. We were able to reasonably fit these cumulative distributions to the shape of the LF$_N$ translocation curves (Fig. 9) using one adjustable dimensionless parameter, Ω, for each curve. This parameter represents the relative importance of drift versus diffusion (Eq. 3). In addition, when Ω = 0, V is ∼40–60 mV (Fig. 10), and because Ω is directly proportional to the drift velocity (Eq. 3), which we supposed to be directly proportional to the driving force, this means that there is an internal driving force arising from an offset voltage of approximately −40 to −60 mV that opposes the movement of LF$_N$ from the cis- to the trans-side.

The number of charges (n) on the Brownian rod requires some further discussion. From the relation of Ω to V (Eq. 4), we calculated that nL/ℓ was between 6 and 9 (Fig. 10). Because the data are from the highly blocked condition, in which each (PA$_{63}$)$_7$ channel has on average about two bound LF$_N$ molecules (Fig. 4), we take L to represent twice the extended length of LF$_N$ (L = ∼2,000 Å).

Using the β-barrel length ℓ = ~100 Å, this gives us n = ~0.3–0.4, a considerably smaller value than expected. (As LF_N gets translocated, there are ~33 residues in the channel [Basilio et al., 2011], which represents one eighth of the 263 residues of LF_N. There are 47 positive residues in LF_N [Bragg and Robertson, 1989], and, as the channel does not admit anions [Basilio et al., 2009], there are on average approximately six positive charges (47/8) in the channel.) Conceivably, the small effective charge could be the result of some sort of counterion screening in the highly confined space around LF_N in the pore, but this seems unlikely given the relatively high cation selectivity of the unblocked pore. Another possibility for obtaining a small effective charge is for the voltage to be dropped across a much smaller distance than the full channel length (e.g., across the Φ clamp). Of course, the linear charge density (n/ℓ) in Eq. 4 does not change and remains a fraction of the value expected from the sequence of LF_N. Curiously, we could obtain more reasonable values for n (between 6 and 9) by using a grossly oversimplified model, with LF_N represented as a Brownian particle that diffuses the length, ℓ, of the β barrel; in this case, ℓ would replace L in Eq. 3 and the factor L/ℓ would disappear from Eq. 4.

We made several simplifying assumptions in constructing our drift-diffusion model. We assumed that LF_N's translocation kinetics are limited by its interaction with the $(PA_{63})_7$ β barrel and, thus, that the relaxation of the polymer segments outside the β barrel is relatively fast. We did not consider details such as the precise charge distribution on the walls of the channel, the specific amino acid sequence of LF_N, or the need to protonate its acidic groups before they can enter the channel. Other theoretical studies of polymer translocation deal explicitly with issues such as the stepwise progression of the polymer through a pore, the flexibility of the polymer chain, and more detailed treatment of frictional effects (Lubensky and Nelson, 1999; Flomenbom and Klafter, 2003; Gauthier and Slater, 2008; Wong and Muthukumar, 2010). As Lubensky and Nelson (1999) have noted, the drift velocity v and diffusion coefficient D in Eq. 2 are phenomenological coefficients that may not obey the simple formulas that we assumed in the Theory section; in particular, both v and D can have a nonlinear dependence on the applied voltage. However, the ratio v/D appears to be relatively insensitive to these deviations, so we doubt that this is a major concern here. Considering the many oversimplifications of this model, its agreement with experimental data are encouraging. The S-shaped kinetics of translocation predicted from the model are in good agreement with experiments (Fig. 9), as is the predicted linear dependence of Ω on voltage (Fig. 10). Even the offset internal negative potential of -40 to -60 mV can be rationalized, given the six heptameric rings of negative residues lining the lumen of the channel (Nassi et al., 2002). On the other hand, there is

no obvious reason why the offset internal potential should be different for WT and His_6-LF_N (Fig. 10). Also, it is surprising that Ω is more positive (6) if only one His_6-LF_N is being translocated at 50 mV (Fig. 8) than if more than one is being translocated (-3; Fig. 9 F), when in fact we would predict the opposite.

A theoretical approach similar to ours has been used to analyze the voltage-dependent escape kinetics of DNA hairpins from the α-hemolysin pore (Wanunu et al., 2008). From the fitted parameters v and D in Table I of Wanunu et al. (2008) and using a polymer length L = ~300 Å, we can calculate Ω, which falls in the range of $1.5-4.0$. Surprisingly, it appears that their Ω decreases as the voltage increases from 10 to 20 mV, rather than increasing as Eq. 4 predicts.

Our drift-diffusion model presents the sequential steps taken by the unwound LF_N chain as it moves down the 100-Å-long β barrel (Fig. 1). Implicit in this is the assumption that the kinetics of LF_N traversing the β barrel are what govern the kinetics of translocation. In particular, we assume that the kinetics of the unfolding of LF_N are rapid in comparison and therefore do not contribute to the kinetics of translocation. (If the kinetics of unfolding and refolding are fast compared with those of translocation, equilibrium essentially exists between the folded and unfolded states, and the probability of being unfolded would affect the absolute timescale of translocation but not the sigmoidal shape of the unblocking curves. Such an equilibrium could also help to explain the remarkably small diffusion coefficients [~10^{-11} cm^2/s] obtained by fitting the drift-diffusion model to the experimental translocation curves.) The exact opposite assumption is taken by Thoren et al. (2009), who feel that it is the unfolding kinetics that govern the translocation kinetics. At this time, it is uncertain which viewpoint is correct. Our observation that the addition of a His_6 tag to the N terminus of LF_N slows translocation (Fig. 11) would appear to favor our assumption because it is unclear how this could affect the unfolding process described by Thoren et al. (2009), whereas one can readily imagine the addition of the 21-residue His_6 tag increasing the interaction of the LF_N chain with the walls of the channel and thereby slowing its progression though the β barrel.

For the drift-diffusion model to fit the experimental translocation curves, we had to choose a diffusion coefficient within the channel of the order of 10^{-11} cm^2/s. This is a very small value and might suggest that our premise that the translocation kinetics are governed by the movement of LF_N through the β barrel is unrealistic. However, this is not the case, as apparently polymer chain movement through a β barrel of dimensions comparable with that of the $(PA_{63})_7$ β barrel is quite slow. For example, translocation of polystyrene sulfonic acid (for which the issue of unfolding of tertiary structure does not exist) through the heptameric β-barrel channel of

α-hemolysin was measured by Wong and Muthukumar (2010). The dimensions of the α-hemolysin β barrel are ~50 Å long and ~20 Å wide (Song et al., 1996), compared with the dimensions of the $(PA_{63})_7$ β barrel of 100 Å long and 15 Å wide. The mean translocation time at an applied voltage of 50 mV for a chain the length of LF_N is ~0.05 s (see Fig. 9 of Wong and Muthukumar, 2010). For the $(PA_{63})_7$ β barrel, which is twice as long and consequently has half the electric field strength at 50 mV than does the hemolysin β barrel, this translates to a mean translocation time of 0.2 s, subject to the conservative assumption that translocation time scales linearly with channel length. (The effective charge of the polystyrene chain within the hemolysin β barrel of ~5 [Wong and Muthukumar, 2010] is comparable with the mean charge of LF_N of ~6 in the $(PA_{63})_7$ β barrel, so we are justified in making the voltage comparisons.) In the narrower $(PA_{63})_7$ β barrel, this time should be even longer. The $t_{1/2}$ of translocation of a single WT LF_N molecule at 50 mV, calculated from 6 s for His_6-LF_N and Fig. 11, is ~3 s. We thus see that it is not unreasonable to believe that it is the interaction of the LF_N chain with the channel that governs the translocation rate.

REFERENCES

Basilio, D., S.J. Juris, R.J. Collier, and A. Finkelstein. 2009. Evidence for a proton-protein symport mechanism in the anthrax toxin channel. *J. Gen. Physiol.* 133:307–314. doi:10.1085/jgp.200810170

Basilio, D., L.D. Jennings-Antipov, K.S. Jakes, and A. Finkelstein. 2011. Trapping a translocating protein within the anthrax toxin channel: implications for the secondary structure of permeating proteins. *J. Gen. Physiol.* 137:343–356. doi:10.1085/jgp.201010578

Benson, E.L., P.D. Huynh, A. Finkelstein, and R.J. Collier. 1998. Identification of residues lining the anthrax protective antigen channel. *Biochemistry.* 37:3941–3948. doi:10.1021/bi972657b

Berezhkovskii, A.M., and I.V. Gopich. 2003. Translocation of rod-like polymers through membrane channels. *Biophys. J.* 84:787–793. doi:10.1016/S0006-3495(03)74898-X

Bragg, T.S., and D.L. Robertson. 1989. Nucleotide sequence and analysis of the lethal factor gene (*lef*) from *Bacillus anthracis. Gene.* 81:45–54. doi:10.1016/0378-1119(89)90335-1

Cunningham, K., D.B. Lacy, J. Mogridge, and R.J. Collier. 2002. Mapping the lethal factor and edema factor binding sites on oligomeric anthrax protective antigen. *Proc. Natl. Acad. Sci. USA.* 99:7049–7053. doi:10.1073/pnas.062160399

Elliott, J.L., J. Mogridge, and R.J. Collier. 2000. A quantitative study of the interactions of *Bacillus anthracis* edema factor and lethal factor with activated protective antigen. *Biochemistry.* 39:6706–6713. doi:10.1021/bi000310u

Finkelstein, A. 2009. Proton-coupled protein transport through the anthrax toxin channel. *Philos. Trans. R. Soc. Lond. B Biol. Sci.* 364:209–215. doi:10.1098/rstb.2008.0126

Flomenbom, O., and J. Klafter. 2003. Single stranded DNA translocation through a nanopore: a master equation approach. *Phys. Rev. E Stat. Nonlin. Soft Matter Phys.* 68:041910. doi:10.1103/PhysRevE.68.041910

Gauthier, M.G., and G.W. Slater. 2008. A Monte Carlo algorithm to study polymer translocation through nanopores. I. Theory and numerical approach. *J. Chem. Phys.* 128:065103. doi:10.1063/1.2826339

Hinkel, J., and R. Mahnke. 2007. Outflow probability for drift–diffusion dynamics. *International Journal of Theoretical Physics.* 46:1542–1561. doi:10.1007/s10773-006-9291-0

Katayama, H., B.E. Janowiak, M. Brzozowski, J. Juryck, S. Falke, E.P. Gogol, R.J. Collier, and M.T. Fisher. 2008. GroEL as a molecular scaffold for structural analysis of the anthrax toxin pore. *Nat. Struct. Mol. Biol.* 15:754–760. doi:10.1038/nsmb.1442

Kintzer, A.F., K.L. Thoren, H.J. Sterling, K.C. Dong, G.K. Feld, I.I. Tang, T.T. Zhang, E.R. Williams, J.M. Berger, and B.A. Krantz. 2009. The protective antigen component of anthrax toxin forms functional octameric complexes. *J. Mol. Biol.* 392:614–629. doi:10.1016/j.jmb.2009.07.037

Krantz, B.A., R.A. Melnyk, S. Zhang, S.J. Juris, D.B. Lacy, Z. Wu, A. Finkelstein, and R.J. Collier. 2005. A phenylalanine clamp catalyzes protein translocation through the anthrax toxin pore. *Science.* 309:777–781. doi:10.1126/science.1113380

Krantz, B.A., A. Finkelstein, and R.J. Collier. 2006. Protein translocation through the anthrax toxin transmembrane pore is driven by a proton gradient. *J. Mol. Biol.* 355:968–979. doi:10.1016/j.jmb.2005.11.030

Lubensky, D.K., and D.R. Nelson. 1999. Driven polymer translocation through a narrow pore. *Biophys. J.* 77:1824–1838. doi:10.1016/S0006-3495(99)77027-X

Melnyk, R.A., K.M. Hewitt, D.B. Lacy, H.C. Lin, C.R. Gessner, S. Li, V.L. Woods Jr., and R.J. Collier. 2006. Structural determinants for the binding of anthrax lethal factor to oligomeric protective antigen. *J. Biol. Chem.* 281:1630–1635. doi:10.1074/jbc.M511164200

Mogridge, J., K. Cunningham, and R.J. Collier. 2002. Stoichiometry of anthrax toxin complexes. *Biochemistry.* 41:1079–1082. doi:10.1021/bi015860m

Mueller, P., D.O. Rudin, H.T. Tien, and W.C. Westcott. 1963. Methods for the formation of single bimolecular lipid membranes in aqueous solutions. *J. Phys. Chem.* 67:534–535.

Nassi, S., R.J. Collier, and A. Finkelstein. 2002. PA_{63} channel of anthrax toxin: an extended β-barrel. *Biochemistry.* 41:1445–1450. doi:10.1021/bi0119518

Neumeyer, T., F. Tonello, F. Dal Molin, B. Schiffler, F. Orlik, and R. Benz. 2006. Anthrax lethal factor (LF) mediated block of the anthrax protective antigen (PA) ion channel: effect of ionic strength and voltage. *Biochemistry.* 45:3060–3068. doi:10.1021/bi0524316

Nguyen, T.L. 2004. Three-dimensional model of the pore form of anthrax protective antigen. Structure and biological implications. *J. Biomol. Struct. Dyn.* 22:253–265.

Pimental, R.A., K.A. Christensen, B.A. Krantz, and R.J. Collier. 2004. Anthrax toxin complexes: heptameric protective antigen can bind lethal factor and edema factor simultaneously. *Biochem. Biophys. Res. Commun.* 322:258–262. doi:10.1016/j.bbrc.2004.07.105

Song, L., M.R. Hobaugh, C. Shustak, S. Cheley, H. Bayley, and J.E. Gouaux. 1996. Structure of staphylococcal alpha-hemolysin, a heptameric transmembrane pore. *Science.* 274:1859–1866. doi:10.1126/science.274.5294.1859

Thoren, K.L., E.J. Worden, J.M. Yassif, and B.A. Krantz. 2009. Lethal factor unfolding is the most force-dependent step of anthrax toxin translocation. *Proc. Natl. Acad. Sci. USA.* 106:21555–21560. doi:10.1073/pnas.0905880106

Wanunu, M., B. Chakrabarti, J. Mathé, D.R. Nelson, and A. Meller. 2008. Orientation-dependent interactions of DNA with an α-hemolysin channel. *Phys. Rev. E Stat. Nonlin. Soft Matter Phys.* 77:031904. doi:10.1103/PhysRevE.77.031904

Wonderlin, W.F., A. Finkel, and R.J. French. 1990. Optimizing planar lipid bilayer single-channel recordings for high resolution with rapid voltage steps. *Biophys. J.* 58:289–297. doi:10.1016/S0006-3495(90)82376-6

Wong, C.T., and M. Muthukumar. 2010. Polymer translocation through alpha-hemolysin pore with tunable polymer-pore electrostatic interaction. *J. Chem. Phys.* 133:045101. doi:10.1063/1.3464333

Young, J.A., and R.J. Collier. 2007. Anthrax toxin: receptor binding, internalization, pore formation, and translocation. *Annu. Rev. Biochem.* 76:243–265. doi:10.1146/annurev.biochem.75.103004.142728

Zhang, S., A. Finkelstein, and R.J. Collier. 2004a. Evidence that translocation of anthrax toxin's lethal factor is initiated by entry of its N terminus into the protective antigen channel. *Proc. Natl. Acad. Sci. USA.* 101:16756–16761. doi:10.1073/pnas.0405754101

Zhang, S., E. Udho, Z. Wu, R.J. Collier, and A. Finkelstein. 2004b. Protein translocation through anthrax toxin channels formed in planar lipid bilayers. *Biophys. J.* 87:3842–3849. doi:10.1529/biophysj.104.050864